Scientia Iranica F (2015) 22(3), 1337–1345

SCIENTIA
IRANICA

Sharif University of Technology
Scientia Iranica
Transactions F: Nanotechnology
www.scientiairanica.com

Evaluation of the effects of nano-TiO_2 on physical and mechanical properties of nano-bioglass 45S5 scaffold for bone tissue engineering

S. Soleymani Eil Bakhtiyari[a], **S. Karbasi**[b,*] **and A. Monshi**[c]

a. *Department of Science and Nuclear Engineering, Najafabad Branch, Islamic Azad University, Najafabad, Isfahan, Iran.*
b. *Biomaterials Group, Advance Medical Technology Department, Isfahan University of Medical Sciences, Isfahan, Iran.*
c. *Department of Material Engineering, Isfahan University of Technology, Isfahan, Iran.*

Received 3 December 2014; received in revised form 17 April 2015; accepted 16 June 2015

KEYWORDS
Nano-bioglass;
Nano-TiO_2;
Scaffold;
Bone tissue engineering.

Abstract. Design of a scaffold with appropriate physical and mechanical properties for tissue engineering is a major challenge. In this research, the effects of nano-titania ($nTiO_2$) on the physical and mechanical properties of a nano-bioglass (nBG) scaffold were evaluated. First, nBG powder with a grain size of 100-110 nm was prepared using the method of melting pure raw material at a temperature of 1400°C. Then, a porous ceramic scaffold of nBG/$nTiO_2$, with 30 wt% of nBG, containing different weight ratios of nano-titania (3, 6 and 9 wt% $nTiO_2$ with a grain size of 35-37 nm), was prepared using the polyurethane sponge replication method. XRD, XRF, SEM, FE-SEM and FTIR were used to study the phase and elemental structures, morphology, particle size, and determination of functional groups, respectively. XRD and XRF results showed that the type of produced bioglass was 45S5. The results of XRD and FT-IR showed that the best temperature to produce a bioglass scaffold was 600°C, because, at this temperature, the crystal was obtained, and the main sign of the obtained crystal was the presence of $Na_2Ca_2Si_3O_9$ crystal. The mechanical strength and modulus of the scaffold improved by adding $nTiO_2$ to the nBG scaffold. The results showed that the scaffolds have 80-88% porosity at the range of 200-600 μm; a compressive strength of 0.04-0.16 MPa, and a compressive modulus of 4-13.33 MPa, illustrating that they could be good candidates for bone tissue engineering.

1. Introduction

Bone is a dynamic, highly vascularized tissue with a unique capacity to heal and remodel without leaving a scar. Bone is a natural composite, and most of its outstanding properties are related to its matrix constitution. Bone matrix has two components; a mineral part consisting of hydroxyapatite, which comprises 65-70% of the matrix, and an organic part, composed of glycoproteins, proteoglycans, sialoproteins and bone “gla” proteins, which comprise the remaining 25-30% of the total matrix [1]. There are roughly 1 million cases of skeletal defects a year that require bonegraft procedures to achieve union [2]. Socioeconomic consequences in treating these patients with bone fractures is a major concern in both the USA and the EU, and this concern will increase in coming years due to the aging of their populations. Current treatments are based on autologous and autogenous bone grafts or, as an alternative to these metal and ceramics [2-6]. Autologous bone graft, i.e. bone taken from another part of the patient’s own body, has been the gold

---

*. *Corresponding author. Tel.: +98 3195016495; Fax: +98 313 6688597*
E-mail address: karbasi@med.mui.ac.ir (S. Karbasi)

standard of bone replacement for many years, as it provides osteogenic cells, as well as essential osteoinductive factors, needed for bone healing and regeneration [5,7]. However, although this type of bone graft presents relatively good success rates, the spectrum of cases in which it can be used is restricted, mainly due to the limited amount of autograft that can be obtained, and donor site morbidity. Thus, the best way to treat bone disorders is the use of tissue engineering [2-6]. Tissue Engineering (TE) is an emerging field that aims to regenerate damaged tissue and/or promote new tissue growth using a combination of cells, biomaterials and signaling molecules [8]. In order to achieve successful regeneration of tissue or organs based on the tissue engineering concept, three critical elements should be carefully considered; biomaterial scaffolds, progenitor cells and growth factors. Biomaterial scaffolds serve as a mechanical support for cell growth, progenitor cells can be differentiated into specific cell types, and growth factors can modulate cellular activities. When tissue is severely damaged or lost, not only are large numbers of functional cells lost, but also the matrix in the tissue, generally called the extracellular matrix (ECM). In tissue engineering, the substitute of native ECM as a "scaffold, "template" or "artificial matrix" is designed. The scaffold provides a three-Dimensional (3-D) ECM analog which functions as a template required for infiltration and proliferation of cells into the targeted functional tissue or organ [9]. Thus, to emulate the bone structure, a porous composite scaffold should be designed. Being similar to the major inorganic component of natural bone, bioceramics, including hydroxyapatite (HAP) and tricalcium phosphate (TCP) [10-12], are widely used as scaffolding materials for bone repair, and these materials have been demonstrated to contain good osteo-conductivity and bone bonding ability [13]. However, the main limitation for the use of ceramics is their inherent brittleness and difficulty of processing [14]. In this research, bioglass was used to fabricate ceramic scaffolds. Bioactive glasses are a subset of inorganic bioactive material, which are capable of reacting with physiological fluids to form tenacious bonds to bone through the formation of bone-like hydroxyapatite layers, and the biological interaction of collagen with the material surface [15]. It has been found that reactions on bioactive glass surfaces lead to the release of critical concentrations of soluble Si, Ca, P and Na ions, which induce favorable intracellular and extracellular responses, leading to a rapid bone formation [16]. However, ceramics are brittle and have low mechanical strength. Montazeri et al. [17] fabricated a ceramic scaffold based on nBG with good bioactivity properties, but with unsuitable mechanical properties. Sirvastava et al. [18] evaluated the bioactivity and physical/mechanical properties of Fe_2O_3 substituted 45S5 bioactive glass. It was observed that an increase in Fe_2O_3 in the base bioactive glass (45S5) results in an increase in its density, micro-hardness and flexural strength. Tubsungneonrattanachan et al. [19] evaluated the effect of adding Zn to apatite/wollastonite glass ceramic scaffolds, showing that the density and compressive strength of the scaffolds decreased with an increase in zinc content. In this research, $nTiO_2$ was added to the nBG scaffold to improve its mechanical strength. TiO_2, also known as titanium oxide, titanium IV oxide or titania, is the naturally occurring oxide of titanium. TiO_2 is a useful material in various applications related to catalysis, electronics, photonics, sensing, medicine and controlled drug release [20]. As nanosized particles, these materials exhibit broad-band UV absorption, a benefit that is currently exploited in sunscreen applications. Also, the addition of nanoparticles would likely enhance the stiffness, toughness and service life of polymeric materials [21]. According to these characteristics, $nTiO_2$ was used to improve the mechanical properties of the nBG scaffold. To the best of our knowledge, this is the first report on the formation of scaffolds from $nBG/nTiO_2$. In this research, the effect of adding different weight ratios of nano titania on the properties of a nBG scaffold prepared by a foam replication method, is shown.

2. Materials and methods

2.1. Preparation of glass powder

Raw materials, including silica, sodium carbonate, calcium carbonate and phosphorus oxides, were mixed together. In order to engage the particles of SiO_2 with each other, these materials were ball-milled for 30 minutes, and to produce a greater amount of nBG powder, the compounds were compressed within the steel frame under pressure. The compressed pieces were then melted in an alumina crucible at a temperature of 1400°C. The resulting melt was drained quickly onto a copper plate. The resultant glass was again ball-milled for 10 hours to produce nBG powder, and then, the produced powder was subjected to XRD, FE-SEM, XRF and FTIR tests.

2.2. Fabrication of ceramic slurry

Preparation of slurry stabilized with proper additives is critical to scaffold formation, and, in this regard, a variety of additives with a range of biological properties has been studied [22]. In this research, a BG scaffold containing different weight ratios of nano-titania (3, 6 and 9 wt%) was produced using a foam replication method. First, 30% (w/v) of nBG was slowly dissolved in double-distilled water to prevent agglomeration. Then, different weight ratios of nano-titania (3, 6 and 9% (w/v) Merck KGaA, 64271, Germany, No 1.00808.1000) were added to the ceramic slurry, and the slurry was stirred at 350 rpm for

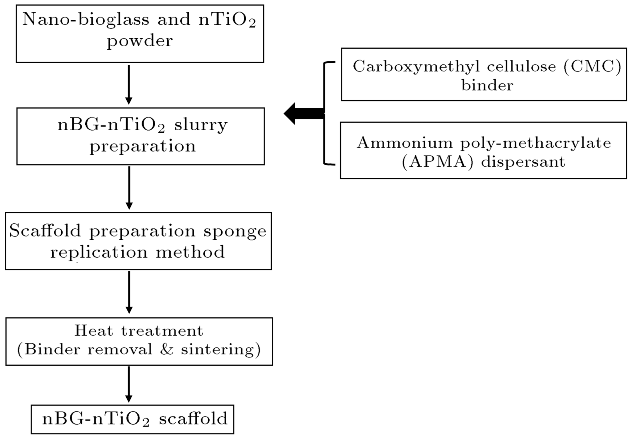

Figure 1. Flow chart of the polymer replication method used for the fabrication of nBG/nTiO$_2$ scaffolds.

90 minutes to produce a homogeneous solution. To maximize the mechanical strength, large amounts of solid material should precipitate from the homogenized solution onto the polyurethane sponge. 2% wt ammonium poly-methacrylate (DARVAN®C-N, R.T. Vanderbilt Company, Norwalk, USA) of the suspension was used to increase the weight percentage of the solid substance. Carboxymethyl cellulose (CMC, Hangzhou Hongbo Chemical Co. Ltd, China) powder (1.5% wt suspension) was slowly added to the solution in order to increase slurry flow and the solution was stirred at 60°C until it became fully homogeneous.

2.3. Preparation of porous scaffold

A commercial polyurethane sponge (MEAY Co., Ltd. China; average pore size of 300-700 μm) was used in this study. The sponge was immersed in ceramic slurry and squeezed twice. Figure 1 shows the flow chart of the polymer replication method used for the fabrication of a Nano-Bioglass/Nano-Titania composite scaffold. The resultant porous body was dried in an oven for 24 hours at 80°C. Subsequently, the scaffolds were placed in a heat treatment furnace. The nBG/nTiO$_2$ composite scaffold was formed in four stages:

1. Treatment at 400°C, with a heating rate of 3°C/min for 1 hour, to completely burn the sponge;
2. An increase in temperature from 400 to 600°C at a rate of 3°C/min;
3. Treatment at 600°C for 4 hours to sinter the ceramic scaffold;
4. Cooling to room temperature at a cooling rate of 5°C/min.

The cooled samples were removed from the furnace, measured, and placed in desiccators. In Figure 2, the left sponge shows the polyurethane sponge before immersion in ceramic slurry, and the right scaffold shows the ceramic scaffold formed at 600°C.

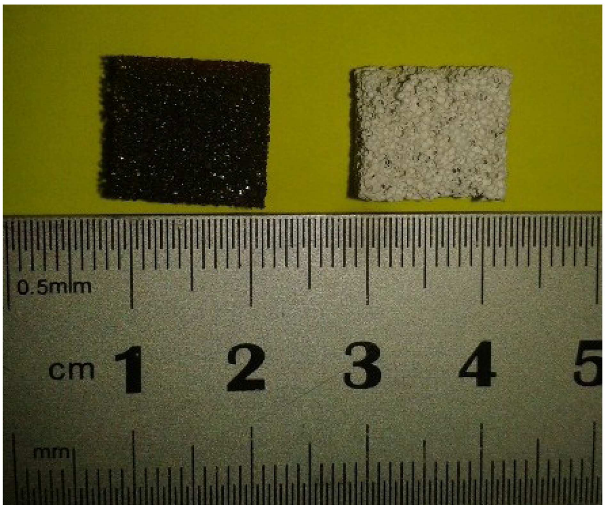

Figure 2. Polyurethane sponge and ceramic porous scaffold after heat treatment in 600°C.

2.4. Physical characterization

2.4.1. X-ray diffraction analysis

X-Ray Diffraction methods (XRD, Philips XPert) were applied to gain information about the structural changes and phases of nBG, nTiO$_2$ and scaffolds. The CuK X-ray was used for analysis. The scan rate was set to 1°/min, the imposed voltage and current were 40 kV and 30 mA, respectively, and the diffraction angle (2θ) varied from 10 to 90°C at a rate of 0.4°/min.

2.4.2. XRF analysis

XRF analysis was used for chemical analysis and for determination of the chemical composition of nBG and nTiO$_2$ powder. Elements with low atomic weight (H$_2$, He and Li) cannot be identified with XRF; however, all the other elements can be identified.

2.4.3. FT-IR spectroscopy

Fourier transform infrared spectroscopy (FT-IR: 6300, JASCO, Japan) was used for studying the functional groups. Spectral analyses were performed using standard Nicolet and Microcal Origin software. FT-IR spectra were taken from nBG powder, nTiO$_2$ powder, nBG scaffold and nBG/nTiO$_2$ scaffold.

2.4.4. Field Emission Scanning Electron Microscopy (FE-SEM)

Field emission scanning electron microscopy (FE-SEM, Philips XL-30, The Netherlands) was used to study the BG nanoparticle. The samples were coated with gold under an argon atmosphere.

2.4.5. Thermal Gravity Analysis (TGA)

Thermal Gravity Analysis (TGA) measures thermal stability and compounding materials. In this research, a thermal gravity analysis device (TG/DTA, TGA 401, Sanatara Co.) was used to record the weight percentage decrease of the polyurethane sponge versus temperature. The sample was heated at a rate of 1°C/min, up to 600°C, under nitrogen flow.

2.4.6. Porosity and density measurements

Liquid displacement was used to calculate the porosity and density of the scaffolds. Scaffold density provides information about the size, distribution and permeability of pores, and the presence of structural defects in sintered ceramic frameworks [23].

Due to the hydrophobic properties of the polymer, 96% ethanol, which can pass easily through pores, was used instead of water. The mass of the ceramic sample (W) was measured, and a volume (V_1) of ethanol was poured into a graduated cylinder and measured. The sample was immersed in ethanol for 5 minutes until it became saturated (V_2). The discrepancy between the volumes (V_1-V_2) represented the volume of the scaffold. The ethanol-soaked scaffold was removed from the graduated cylinder, and the remaining volume was recorded as V_3. V_1-V_3 represented the volume of ethanol absorbed by the scaffold [22].

The following equation calculates the density of the scaffold (ρ):

$$\rho = \frac{W}{V_2 - V_3}. \tag{1}$$

The following equation calculates the amount of open porosity of the scaffold (ε):

$$\rho = \frac{V_1 - V_3}{V_2 - V_3}. \tag{2}$$

2.4.7. Scanning Electron Microscopy (SEM)

Scanning electron microscopy (SEM, Philips XL-30, The Netherlands) was used to study the morphology of nBG powder and scaffolds. The samples were coated with gold under an argon atmosphere.

2.5. Mechanical characterization

Machining and gripping the specimen is a major problem in the mechanical characterization of porous ceramic scaffolds. Conventional methods of mechanical characterization, such as tensile, biaxial and impact tests are usually inapplicable to porous materials [23]. Compression impact tests for porous bone and nBG samples are instead used [22-25]. Compressive strength and compressive module tests for samples with and without $nTiO_2$ were performed using a compression impact tester (SANTAM- Eng. Design Co. LTD) with a 10-kN load cell, based upon guidelines set in ASTM-D5024-95a. The dimensions of each sample were 20 × 10 × 10 mm^3 for the compression impact test. As ceramic scaffolds are fragile, the crosshead speed was set at 0.5 mm/min to prevent damage to the ceramic structure. The load carried by the sample was considered to be 30% of the scaffold's original length. The elastic modulus was calculated as the slope of the initial linear portion of the stress-strain curve. The yield strength was determined from the cross point of the two tangents on the curve around the yield point.

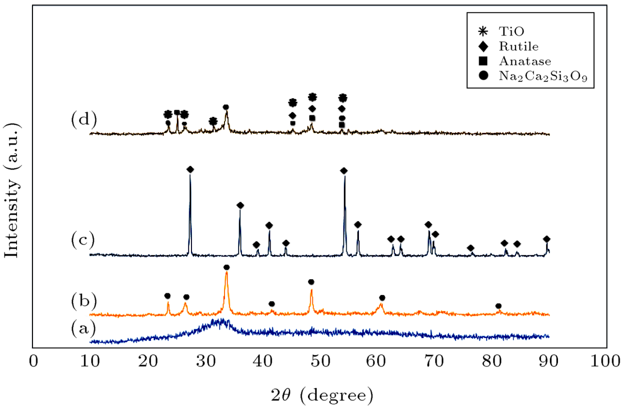

Figure 3. Pattern of XRD analysis: (a) 45S5 nBG powder made at 1400°C; (b) bioglass scaffold at 600°C; (c) $nTiO_2$ powder; and (d) nBG/$nTiO_2$ scaffold at 600°C.

3. Results and discussion

3.1. nBG, $nTiO_2$, bioglass scaffold and nBG/$nTiO_2$ composite scaffold

3.1.1. X-ray diffraction analysis

Figure 3(a) shows x-ray diffraction spectra wherein the 45S5 nBG powder was produced by the melting method. According to the XRD spectra, it is obvious that the obtained product was bioglass, because no additional stable phase and sharp peak were found [26]. This could be the result of the fact that this combination is devoid of any crystalline phase, but only has a glass halo between a 20 and 40 degree angle. This sign confirms the amorphous structure of bioglass powder. In Figure 3(b), by making a solution and constructing scaffolding at 600° C, peak XRDs are shown. In the XRD spectra of the bioglass scaffold, a sharp peak was found at a 32.575° angle, which is related to $Na_2Ca_2Si_3O_9$ crystal. Figure 3(c) shows the XRD of the pure $nTiO_2$ powder sample.

Peaks at 27.51°, 36.15°, 39.31°, 41.30°, 44.13°, 54.37°, 56.69°, 62.77°, 64.09°, 69.04°, 69.78°, 76.6°, 82.37°, 84.34° and 89.55° angles were observed, confirming the formation of the rutile phase of $nTiO_2$. Figure 3(d) shows the XRD of the nBG/$nTiO_2$ composite scaffold sample. The peaks at 23.76° and 26.6° angles were related to $nTiO_2$ with unknown crystalline structures and a $Na_2Ca_2Si_3O_9$ crystalline phase. The observed peaks at 25.3°, 31.6° and 33.84° angles were related to anatase and $nTiO_2$, with an unknown crystalline structure and $Na_2Ca_2Si_3O_9$ crystalline phase, respectively. The peak at a 45.4° angle was related to rutile, anatase and $nTiO_2$, with an unknown crystalline structure. The peak observed at 48.62° was related to $nTiO_2$, with an unknown crystalline structure,

Table 1. Chemical analysis of nano-bioglass powder.

Compound	**Concentration (%W/W)**
SiO_2	42.92
CaO	25.86
Na_2O	18.20
Al_2O_3	3.35
P_2O_5	1.87
MgO	0.100
Fe_2O_3	0.095
SO_3	0.048
CuO	0.023
LOI*	**7.38**
Total	**99.85**

$Na_2Ca_2Si_3O_9$ crystalline and rutile phase. The peak at 53.8° showed all the mentioned phases. The results of XRD showed that, according to the JCPDS 033-1161 standard, the scaffold was composite, because the main peaks of TiO_2 were observed in the nBG/nTiO_2 composite scaffold. The sizes of the crystals of bioglass, TiO_2 and NBG/NTiO_2 scaffolds were obtained by a modified Scherrer equation [27]. The sizes of the crystals of nTiO_2, with an unknown crystalline structure, rutile phase, $Na_2Ca_2Si_3O_9$ crystalline phase and anatase, were 28, 23, 17 and 46 nm, respectively.

3.1.2. XRF analysis

The results of XRF analysis of the nBG powder sample produced using the melting method are presented in Table 1, which shows, with acceptable matching, that the weight percentages are similar to standard weight percentages of 45S5. These results confirmed the production of bioglass with favorable weight percentages (45S5) [28]. A chemical analysis of nTiO_2 powder is presented in Table 2.

3.1.3. FT-IR spectroscopy

The patterns of FT-IR bioactive glass 45S5 powder and bioactive glass ceramic scaffold are shown in Figure 4(a) and (b), respectively. Figure 4(a) shows the FTIR diagram related to the bioactive glass 45S5 powder in which peaks of 506,936 and 1014 cm^{-1} are related to the stretching vibration of Si-O-Si, SiO, and the bending vibration of Si-O-Si, respectively. The absorption band at 697 cm^{-1} is related to amorphous phosphate. The 1453 cm^{-1} band in the spectra of the bioactive glass 45S5 is related to the organic components. The strong peaks visible at 1634 and 3444 cm^{-1} are attributed to the hydroxyl group. The pattern of FTIR also shows that the polyurethane foam used in the preparation of the scaffold during the heating process was completely out of the system. In Figure 4(b), the sharp peaks at 457 and 519 cm^{-1} are due to the P-O bending vibration. The peaks visible at 618 and 3442 cm^{-1} were related to the stretching vibration of O-H. The absorption band at 1438 cm^{-1} was attributed to the stretching vibration of the carbonate group. The sharp peaks at 922 and 1032 cm^{-1} were related to Si-O stretching vibration and Si-O-Si bending vibration, respectively. The absorption band at 695 cm^{-1} was related to the amorphous phosphate. A recent infrared analysis carried out by Boskey and Camacho [29] revealed that the main mineral components of bone are phosphate and carbonate, which are related to hydroxyapatite, and a series of absorption bands are related to amide groups that are related to proteins (collagen) in the bone, with absorption bands occurring in the range between 800 cm^{-1} and 1800 cm^{-1} [29]. In this research, the main mineral component of bone was observed in the FTIR of the nBG scaffold, so, it can be concluded that this nBG scaffold has a similar structure to bone.

Table 2. Chemical analysis of nano-TiO_2 powder.

Compound	**Concentration (%W/W)**
TiO_2	99.33
Al_2O_3	0.18
ZrO_2	0.004
SiO_2	0.110
P_2O_5	0.110
SO_3	0.058
CaO	0.056
CuO	0.034
Nb_2O_5	0.024
Fe_2O_3	0.020
ZnO	0.017
K_2O	0.013
LOI*	
Total	**99.96**

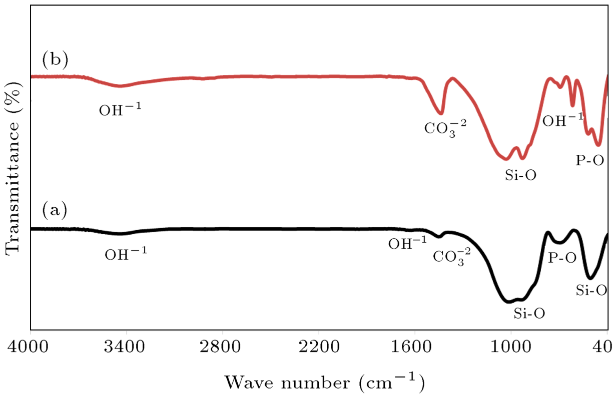

Figure 4. Pattern of FT-IR analysis: (a) Bioglass powder; and (b) porous ceramic scaffold at 600°C.

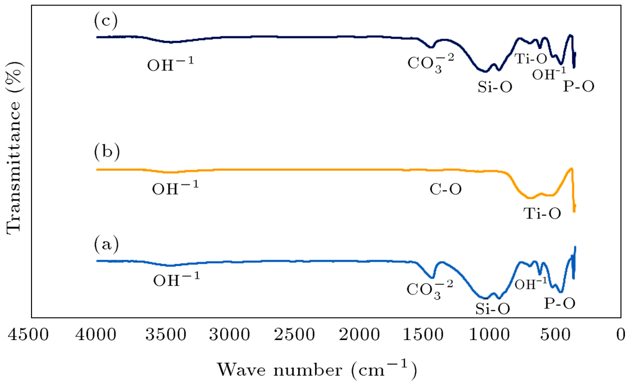

Figure 5. Pattern of FT-IR analysis: (a) Porous ceramic scaffold at 600°C; (b) $nTiO_2$ powder; and (c) $nBG/nTiO_2$ scaffold at 600°C.

The patterns of the FT-IR bioactive glass ceramic scaffold, $nTiO_2$ powder and $nBG/nTiO_2$ scaffold are shown in Figure 5(a), (b) and (c). The pattern of FTIR in Figure 5(a) indicates the process mentioned in Section 3.1.3 (Figure 4(b)), regarding the FTIR of the nBG scaffold. In Figure 5(b), related to the FTIR diagram of the $nTiO_2$ powder, the absorption bands emerge at 538 and 690 cm^{-1}, due to the vibration of Ti-O-Ti in the TiO_2 lattice. The 1632 cm^{-1} peak in the spectra of the $nTiO_2$ powder was related to H_2O absorption and the bending vibration of H-O-H. The peaks at 1105 and 1424 cm^{-1} were attributed to the vibration of C-O. The strong peak at 3434 cm^{-1} was due to the stretching vibration of hydroxyl groups. In Figure 5(c), the FT-IR spectra of the $nBG/nTiO_2$ scaffold have different absorption bands and these regions include sharp peaks related to the nBG scaffold and $nTiO_2$ powder. The peaks at 458 and 516 cm^{-1} were due to the bending vibration of P-O, and these similar peaks were also visible in the FTIR of the NBG scaffold. Strong peaks at 618 and 3433 cm^{-1} were related to the stretching vibration of hydroxyl groups. The peak at 697 cm^{-1} was related to the overlap of two peaks related to the amorphous phosphate of the nBG scaffold and the vibration of Ti-O-Ti in the TiO_2 lattice and in the FTIR of $nBG/nTiO_2$ composite scaffold. The intensity of the peak visible at 690 cm^{-1}, related to the vibration of Ti-O-Ti in the TiO_2 lattice, decreased, because the amount of $nTiO_2$ added to the nBG scaffold was low. The peak at 1443 $cm^{-1}$was attributed to the stretching vibration and impurities of carbonate. The results of FTIR showed that adding $nTiO_2$ to the nBG scaffold shifted the peak of the absorption band attributed to the stretching vibration of the carbonate group from 1438.64 cm^{-1} to 1443.46 cm^{-1}. According to the results of FTIRs, it can be concluded that adding $nTiO_2$ to the nBG scaffold shifted the peak of the stretching vibration of the carbonate group from 1438.64 cm^{-1} to 1443.46 cm^{-1}, and this event can be a good reason for an increase in compressive strength.

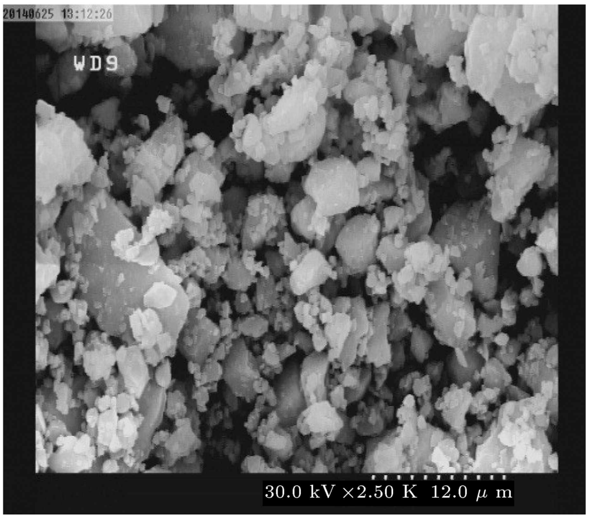

Figure 6. FE-SEM of nano-bioglass powder.

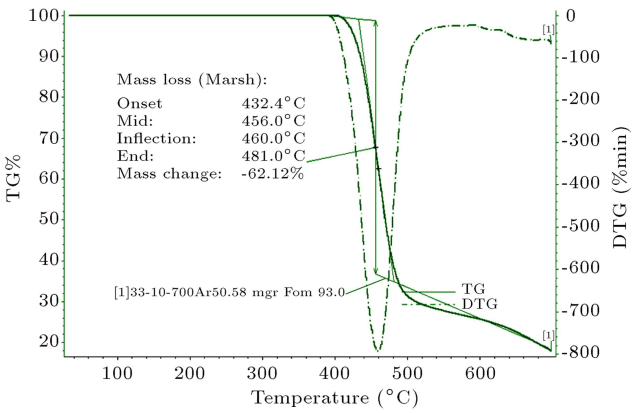

Figure 7. Weight loss as a function of temperature (heating rate=3°C/min) for pyrolysis of polyurethane sponge.

3.1.4. Field Emission Scanning Electron Microscopy (FE-SEM)

Figure 6 shows that the particles mainly had a semi-spherical morphology with a particle size of about 100-110 nm.

3.1.5. Thermal Gravity Analysis (TGA)

In order to prevent cracks in the ceramic structure, there should be sufficient time for the burning of polymeric foams. Figure 7 shows the weight change of the polyurethane foam relative to temperature. The figure shows that the main part of the polymer was removed at temperatures between 380°C and 600°C. It is, therefore, necessary to take into account the slow heating rate at this stage to prevent structural damage caused by emissions from the thermal degradation of polymers. At temperatures above 600°C, the polymer foam had a low weight decrease, due to the amount of carbon produced from the decomposition of the polymer process dioxide. Complete combustion of polymeric foams occurred at 600°C.

Table 3. Porosity percentage of nBG scaffold with and without $nTiO_2$.

Sample	Mean porosity (%)
S_1	88%
S_2	86%
S_3	83%
S_4	80%

S_3: BG-6% $nTiO_2$ scaffold;

S_4: BG-9% $nTiO_2$ scaffold.

3.1.6. Porosity and density measurements

The porosity measurement was performed on the nBG scaffold, with and without $nTiO_2$, and the porosity was between 80-88%. The results of the porous percentage of the samples are shown in Table 3. The results showed that $nTiO_2$ did not have a bad effect on the porosity of samples, and there was good interconnectivity between the pores.

3.1.7. Scanning Electron Microscopy (SEM)

Figure 8(a) shows the electron microscopic images of polyurethane foam with open pores, within a range of 300-700 μm, before immersion in the ceramic slurry. Figure 8(b) shows the porous nano-bioglass scaffold. Figure 8(c) and (d) show the porous nBG/$nTiO_2$ scaffold, with pore diameters ranging from 200 to 600 μm. Porosity and interconnectivity are important for accurate diffusion of nutrients and gases, and for the removal of metabolic waste resulting from the activity of cells that have meanwhile grown into the scaffold [30]. In these samples, the interconnectivity between pores was preserved.

Table 4. Comparison between porosity percentage, compressive strength and compressive modulus of nBG scaffold with and without $nTiO_2$.

Sample	Mean porosity (%)	Compressive strength (MPa)	Compressive modulus (MPa)
S_1	88%	0.04 ± 0.01	4 ± 0.2
S_2	86%	0.07 ± 0.02	5.83 ± 0.3
S_3	83%	0.1 ± 0.01	8.33 ± 0.2
S_4	80%	0.16 ± 0.02	13.33 ± 0.2

S_1: BG Scaffold; S_2: BG-3% $nTiO_2$ scaffold;

S_3: BG-6% $nTiO_2$ scaffold; S_4: BG-9% $nTiO_2$ scaffold.

3.2. Compressive strength of bioglass scaffold with and without TiO_2

The compressive strength test was performed on the nBG scaffold, with and without $nTiO_2$, and the results are shown in Table 4. The results of compressive strength show that the compressive strength in nBG scaffolds without $nTiO_2$ was 0.04 MPa, while the compressive strength in the nBG/$nTiO_2$ composite scaffold was higher. Table 4 also shows that by adding $nTiO_2$ to the bioglass scaffold, the strength and modulus increase. Callcut et al. [31] showed that a compressive strength of 0.01-0.175 MPa can be achieved using the polymeric sponge method with a reinforced hydroxyapatite coating of glass. Chen et al. [32] produced scaffolds from bioactive glass coated with a polymer PDLLA; the compressive strength of the scaffold before coating was 0.045 MPa. A comparison between the fabricated scaffolds in this research with the fabricated scaffold by Chen et al. show that

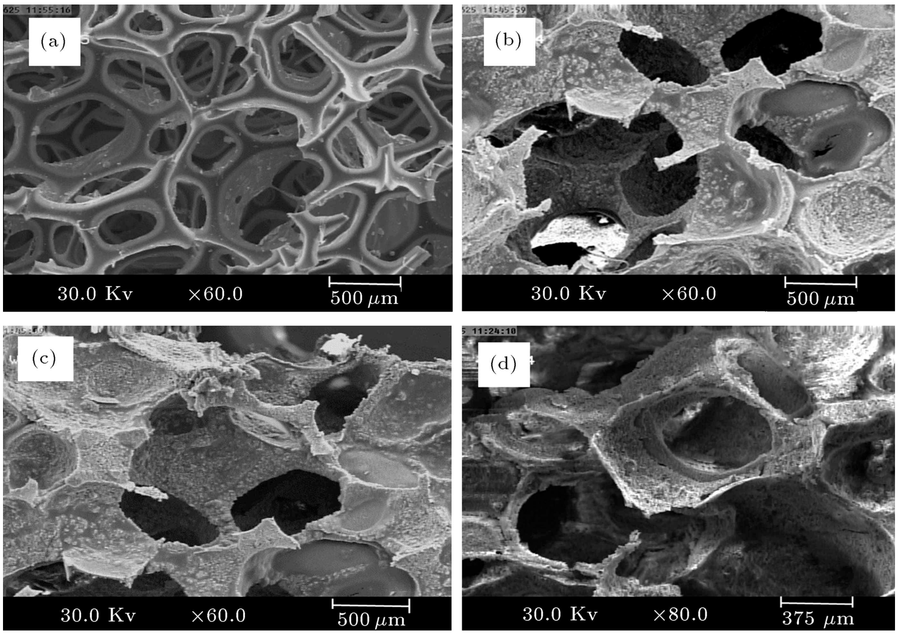

Figure 8. (a) Polyurethane sponge's image captured by SEM (60x). (b) Cross section of nBG scaffold without $nTiO_2$. (c) and (d) Cross section of nBG scaffold with $nTiO_2$.

the bioglass scaffold has a compressive strength of nearly 0.04 MPa. However, by adding $nTiO_2$ to the bioglass scaffold, its compressive strength increases. Since bioglass has no grain boundary, it cannot stop the progress of a crack. According to the Grifith theory, maximum stress develops at the tip of the crack from applied stress. This high amount of stress at the crack tip causes the rapid propagation of crack and the failure of the body. In glass ceramics, some nucleation of phases is performed inside the matrix, so that these phases with a grain boundary can impede or stop the crack progress. In glass ceramics, the presence of 1-2% TiO_2 is very useful to act as the nucleation agent of the phases. The TiO_2 particles act as a base for nucleation of the phase by heterogeneous nucleation [33,34]. In this study, the presence of 6% of TiO_2 has provided adequate nuclei for the development of phases in bioglass and for increasing the strength, respectively.

4. Conclusion

In this research, a ceramic scaffold, with 30 wt% of nBG and 3,6 and 9 wt% of $nTiO_2$, was prepared using a polyurethane sponge replication method. FTIR, XRD and XRF results showed that the type of produced bioglass was 45S5. It can be proven that the composite structure was a composite scaffold of $nBG/nTiO_2$ with 0.04-0.16 MPa compressive strength and 80-88% porosity. Therefore, this scaffold has good potential for bone tissue engineering applications.

References

1. Sommerfeldt, D.W. and Rubin, C.T. "Biology of bone and how it orchestrates the form and function of the skeleton", *Eur. Spine J.*, **10**(2), pp. 86-95 (2001).
2. Yaszemski, M.J., Oldham, J.B., Lu, L. and Currier, B.L., *Bone Engineering*, 1st Ed., Em squared, Toronto (2000).
3. Spitzer, R., Perka, C., Lindenhayn, K. and Zippel, H. "Matrix engineering for osteogenic differentiation of rabbit periosteal cells using -tricalcium phosphate particles in a three-dimensional fibrin culture", *J. Biomed. Mat. Res.*, **59**(4), pp. 690-696 (2002).
4. Simon, G.C., Khatri, C.A., Wight, S.A. and Wang, F.W. "Preliminary report on the biocompatibility of a moldable, resorbable, composite bone graft consisting of calcium phosphate cement and poly(lactide-co-glycolide) microspheres", *J. Orthop. Res.*, **20**(3), pp. 473-482 (2002).
5. Rose, F.R. and Oreffo, R.O. "Bone tissue engineering: hope vs hype", *Bioch. and Bioph. Res. Comm.*, **292**(1), pp. 1-7 (2002).
6. Petite, H., Viateau, V., Bensaid, W., Meunier, A., de Pollak, C., Bourguignon, M., Oudina, K., Sedel, L. and Guillemin, G. "Tissue-engineered bone regeneration", *Nat. Biotech.*, **18**(9), pp. 959-963 (2000).
7. Asahina, I., Seto I., Oda, M., Marukawa, E., Imranul, A.M. and Enomoto, S., *Bone Engineering*, 1st Ed., Em squared, Toronto (2000).
8. Langer, R. and Vacanti, J.P. "Tissue engineering", *Science.*, **260**(5110), pp. 920-6 (1993).
9. Ikada, Y., *Tissue Engineering: Fundamentals and Applications*, Elsevier Ltd, The Boulevard, Langford Lane Kidlington, pp. 1-2, Oxford, UK (2006).
10. Flautre, B., Descamps, M., Delecourt, C., Blary, M.C. and Hardouin, P. "Porous HA ceramic for bone replacement: Role of the pores and interconnections-experimental study in the rabbit", *J. Mater. Sci. Med.*, **12**, pp. 679-682 (2001).
11. Li, S.H., deGroot, K. and Layrolle, P. "Bioceramic scaffold with controlled porous structure for bone tissue engineering", *Key Eng. Mater.*, **218-220**, pp. 25-30 (2002).
12. Sun, J.S., Liu, H.C., Chang, W.H.S., Li, J., Lin, F.H. and Tai, H.C. "Influence of hydroxyapatite particle size on bone cell activities: an in vitro study", *J. Biomed. Mater. Res.*, **39**, pp. 390-397 (1998).
13. LeGeros, R.Z. "Properties of osteoconductive biomaterials: calcium phosphates", *Clin. Orthop. Relat. Res.*, **395**, pp. 81-98 (2002).
14. Cooke, F.W. "Ceramics in orthopedic surgery", *Clin. Orthop.*, **276**, pp. 135-146 (1992).
15. Hench, L.L. "Bioceramics", *J. Am. Ceram. Soc.*, **81**, pp. 1705-1728 (1998).
16. Xynos, I.D., Edgar, A.J., Buttery, L.D.K., Hench, L.L. and Polak, M. "Gene expression profiling of human osteoblasts following treatment with the ionic products of BioglassR 45S5 dissolution", *J. Biomed. Mater. Res.*, **55**, pp. 151-7 (2001).
17. Montazeri, M., Karbasi, S., Forough, M.R., Monshi, A., Ebrahimi-Kahrizsangi, R. "Evaluation of mechanical property and bioactivity of nano-bioglass 45S5 scaffold coated with poly-3-hydroxybutyrate", *J. Mat. Sci. Mat. Med.*, **26**, pp. 62-72 (2015).
18. Sirvastava, A.K., Pyare, R. and Singh, S.P.?? "In vitro bioactivity and physical - mechanical properties of Fe_2O_3 substituted 45S5 bioactive glasses and glass - ceramics", *Int. J. Sci. Eng. Res.*, **3**(2), pp. 1-15 (February, 2012).
19. Tubsungneon Rattanachan, S., Srakaew, N.L., Pethnin, R. and Suppakarn, N. "Effect of Zn addition on sol-gel derived apatite/wollastonite glass-ceramics scaffolds", *J. Metals. Mater. and Minerals*, **22**(2), pp. 61-65 (2012).
20. Wang, W., Gu, B., Liang, L., Hamilton, W.A. and Wesolowski, D.J. "Synthesis of rutile (α-TiO_2) nanocrystals with controlled size and shape by low-

temperature hydrolysis: Effects of solvent composition", *J. Phys. Chem. B.*, **108**(147), pp. 89-92 (2004).

21. Hema, M., Yelilarasi, A., Tamilselvi, P. and Anbarasan, R. "Titania nanoparticles synthesized by sol-gel technique", *Chem. Sci. Trans.*, **2**(1), pp. 239-245 (2013).
22. Ramay, H. and Zhang, M. "Preparation of porous hydroxyapatite scaffolds by combination of the gel-casting and polymer sponge methods", *Biomaterials.*, **24**, pp. 3293-3302 (2003).
23. Hodgskinson, R. and Currey, J.D. "Effect of variation in structure on Young's modulus of cancellous bone", *J. Eng. Med.*, **204**, pp. 115-121 (1986).
24. Curry, J.D. "The mechanical properties of bone", *Clin. Orthop. Rel. Res.*, **73**, pp. 210-231 (1970).
25. Hing, K.A., Best, S.M. and Bonfield, W. "Characterization of porous hydroxyapatite", *J. Mater. Sci.*, **10**, pp. 135-145 (1999).
26. Hench, L.L. "The story of bioglass", *J. Mater. Sci.*, **17**, pp. 967-978 (2006).
27. Monshi, A., Foroughi, M.R. and Monshi, M.R. "Modified scherrer equation to estimate more accurately nano-crystallite size", **2**, pp. 154-160 (2012).
28. Qizhi Chen, Z., Ian Thompson, D. and Aldo Boccaccini, R. "45S5 bioglass-derived glass ceramic scaffolds for bone tissue engineering", *Biomaterials.*, **27**, pp. 2414-2425 (2006).
29. Boskey, A. and Camacho, N. "FT-IR imaging of native and tissue engineered bone and cartilage", *Biomaterials.*, pp. 2465-2478 (2006).
30. Freed, L.E. and Vunjak-Novakovic, G. "Culture of organized cell communities", *Adv. Drug. Deliv. Rev.*, **33**(1-2), pp. 15-30 (1998).
31. Callcut, S. and Knowles, J.C. "Correlation between structure and compressive strength in a reticulate glass-reinforced hydroxyapatite foam", *J. Mater. Sci. Mater. Med.*, **13**, pp. 485-489 (2002).
32. Chen, Q.Z. and Boccaccini, A.R. "Poly(DL-lactide) coated 45S5 bioglass-based scaffolds: Processing and characterization", *J. Biomed. Mater. Res.*, **77**, pp. 445-452 (2006).
33. Salama, S.N., Salman, S.M. and Darwish, H. "The effect of nucleation catalysts on crystallization characteristics of aluminosilicate glasses", *Ceramics.*, **46**(1), pp. 15-23 (2002).
34. Rezvani, M. "Effects of various nucleation agents on crystallization kinetic of LAS glass ceramic", *Iranian. J. Mater. Sci.* & *Eng.*, **8**(4), pp. 41-49 (2011).

Biographies

Sanaz Soleymani Eil Bakhtiyari received her BS degree in Ceramic-Material Engineering from Shahreza Islamic Azad University, Iran, in 2012, and her MS degree in Tissue Engineering from Najafabad Islamic Azad University, Iran, in 2014. She is currently pursuing research in tissue engineering.

Saeed Karbasi received his BS degree in Material Engineering from Shiraz University, Iran, in 1994, and MS and PhD degrees in Biomedical Engineering from Amirkabir University, Iran, in 1997 and 2005, respectively. He is currently Associate Professor at Isfahan University of Medical Sciences, Iran. His research interests include biomaterials, tissue engineering and nanobiomaterials.

Ahmad Monshi obtained his MS degree in Metallurgy from Shiraz University, Iran, in 1978, and a PhD degree in Ceramics Engineering from Sheffield University, UK, in 1990. He was selected as one of the 2000 outstanding scientists of the 20th century by the International Biographic Center in Cambridge, UK, in 2000, and obtained an International Diploma of Honor from the Biographical Center, USA, in 2001. His research interests include biomaterials, nanomaterials, analytical methods, especially XRD, solidification and advanced materials.